Geophys. J. R. astr. Soc. (1974) **36**, 515–539.

The Structure of the Upper Mantle under the United States from the Dispersion of Rayleigh Waves*

N. N. Biswas† and L. Knopoff

(Received 1973 October 4)‡

Summary

Seismograms from vertical-component, long-period instruments of the World-Wide Standard Seismographic Network (WWSSN) within the United States have been analysed to determine the dispersion of Rayleigh waves by the two-station method. Phase velocities from fundamental mode Rayleigh waves over the period range 20–250 s have been obtained to study the structure of the upper mantle of the continent. The phase velocities show systematic variations in specific sub-regions of the United States. The phase velocities observed along five representative paths have been inverted into sub-surface structural cross-sections by the Hedgehog method. The results of the inversion indicate that there are significant regional variations in *S*-wave velocities, particularly from the Moho down to about 400 km. We make no statement about lateral variations in structure at greater depths. The aseismic south-central part of the continent and the tectonically active western Cordillera are characterized by a well-developed low-velocity channel for *S* waves in the upper mantle. The north-central United States has dispersion data which are consistent with structures which either have a low velocity channel of marginal properties or no low velocity channel at all; if a channel is present for this region, the velocity contrast with the layers of the mantle above and below it is very small.

1. Introduction

Dorman's (1969) summary of surface wave dispersion data in the period range 20–300 s shows significant variation of the dispersion characteristics not only between oceans and continents but within a continent as well. The presence of a large scale lateral variation of Rayleigh wave dispersion in the United States was first shown by Pilant (1967). He provided phase velocity contour maps for the entire United States in the period range of 20–51 s. A prominent feature of these maps is a low-velocity region under the Basin–Range province and a sharp gradient across the northern Rockies.

* Publication Number 1198, Institute of Geophysics and Planetary Physics, University of California, Los Angeles.

† Present address: Geophysical Institute, University of Alaska, College, Alaska.

‡ Received in original form 1973 May 7.

Downloaded from https://academic.oup.com/gji/article/36/3/515/585195 by guest on 21 August 2022

Dorman & Ewing (1962), using the two-station method, obtained the crust–upper mantle structure in the New York–Pennsylvania area from Rayleigh wave data. Their phase velocity data extend only up to a period of 46 s. McEvilly (1964) used Rayleigh and Love wave phase velocities in the period range of 5–80 s for structural studies in the central United States, also by the two-station method. These studies were confined to relatively short-period data; thus, the structural details of the upper mantle obtained from the inversions have considerable uncertainties.

To obtain dispersion information at longer periods, Toksöz & Ben-Menahem (1963), and Toksöz & Anderson (1966) determined Love and Rayleigh wave phase velocities over the period range 100–600 s for great-circle circuits of the Earth from large earthquakes, recorded in the United States. Toksöz & Anderson (1966) classified the regions traversed by the great circle paths into oceans, tectonic areas and shields. The percentage of the total path included in each region was determined geographically. The models proposed for the above three structural provinces show significant differences in *S*-wave velocities, especially in the upper mantle.

From the analysis of seismograms taken from multiple circuits of the Earth along great circles, Kanamori (1970) obtained phase and group velocities of Love and Rayleigh waves from a large body of data in the period range of about 150–325 s. He proposed two upper mantle models, 5·08 M and 5·08 TECT, for the ocean and tectonically active regions respectively, which were modifications of model 5·08 of Press (1969), and designed to fit pure-path oceanic and tectonic data.

Dziewonski (1971a) followed the same approach as Kanamori: he reduced his data using the group velocity filtering technique of Dziewonski & Landisman (1970). Assuming identical Rayleigh wave dispersion within a certain range of azimuths measured at the epicentre, he obtained phase and group velocities corresponding to ocean, shield and tectonic regions. Dziewonski sampled about 33 per cent of the Earth's surface, and thereby covered a relatively larger percentage of the tectonic and shield portions of the Earth than Kanamori (1970). Dziewonski (1971b) derived models of the upper mantle for oceanic (O1), tectonic (T1) and shield (S1 and S2) regions which show considerable variations in *S*-wave velocity from one to the other, a feature also noted by earlier workers. There are systematic differences between Dziewonski's and Kanamori's phase velocities.

The results obtained from great-circle passages are not representative of any particular ocean, shield or tectonic province. Instead they represent the averages of a variety of each of the three types of structural provinces (Dziewonski 1971b). Knopoff (1972) has discussed in detail the advantages of pure-path regional studies compared with ' great circle decomposition ' methods.

In view of these facts, we have studied Rayleigh wave dispersion in the continental United States in order to test the validity of the subdivision of this continental region into only two subdivisions, ' shield ' and ' tectonic '. Broadly, the United States is known to be marked by different structural provinces for which fairly detailed cross-sections of *P*-wave velocities in the crust and uppermost mantle are available from explosion studies. It is of interest to see whether these lateral inhomogeneities extend to greater depths, and, if so, how.

2. Data

The seismograms analysed in this study were recorded by WWSSN stations located within the United States. The list of stations is given in Table 1. The events are in the range of USCGS magnitudes 5·3–6·5 and have shallow focal depths. These records have large well-developed surface wave trains and are on scale in all cases.

To overcome the difficulties of determining the initial phase of the source which

Downloaded from https://academic.oup.com/gji/article/36/3/515/585195 by guest on 21 August 2022

is encountered in the single-station phase velocity measurements (Knopoff & Schwab 1968), we have used the two-station method in this study. In this method, under the assumption that the angle between the great-circle path between the earthquake and the stations on the one hand and the great-circle connecting the stations on the other hand is small, the effect of the initial phase of the source is eliminated.

We have analysed only the Z-component records of each station pair. In choosing the seismic events, it has been found that a significant difference between the epicentral and interstation great-circle paths yielded phase velocities with large scatter, a feature also noted by Brune & Dorman (1963). This can probably be attributed to lateral heterogeneity (Knopoff, Berry & Schwab 1967). We restricted our study to only those records for each path for which the angular difference between the epicentral and station-pair paths did not exceed 7°.

We only used R1 in this study and thereby avoided the possibility of large changes in direction of arrival on later passes due to multiple continent-ocean refractions (Madariaga & Aki 1972). The two-station method was first used by Brune & Dorman (1963) with peak-and-trough analysis and subsequently with machine Fourier analysis by Knopoff, Mueller & Pilant (1966).

Table 1

List of stations and earthquake epicentres

Stations	
AAM	Ann Arbor, Mich.
BKS	Byerly, Calif.
BOZ	Bozeman, Mont.
DUG	Dugway, Utah
FLO	Florissant, Mo.
GOL	Golden, Colo.
GSC	Goldstone, Calif.
LON	Longmire, Wash.
LUB	Lubbock, Tex.
MDS	Madison, Wisc.
MNN	Minneapolis, Minn.
OGD	Ogdensburg, N.J.
OXF	Oxford, Miss.
SHA	Spring Hill, Ala.
TUC	Tucson, Ariz.

		Epicentres			
Path	Date	Origin time	Lat.	Long.	Station pair
1	1966 Sept. 2	07:59:05	4·5° S	106·1° W	GSC–LON
2	1965 Aug. 20	21:21:52	22·8 S	176·2 W	BKS–BOZ
3	1964 Oct. 12	21:55:33	31·3 S	110·8 W	TUC–BOZ
4	1965 Nov. 15	11:18:50	0·3 S	18·6 W	GOL–DUG
5A	1964 Sept. 19	05:08:15	15·3 N	94·0 W	LUB–GOL
5B	—	—	—	—	GOL–BOZ
6	1964 Sept. 16	22:23:36	22·9 N	45·1 W	FLO–GOL
7	1964 July 9	11:22:05	23·3 S	175·7 W	GOL–MNN
8	1964 Sept. 17	15:02:01	44·5 N	31·3 W	MNN–GOL
9A	—	—	—	—	AAM–FLO
9B	—	—	—	—	FLO–LUB
10	1965 Nov. 16	15:24:43	31·0 N	41·5 W	OXF–LUB
11	1965 June 2	23:40:24	15·9 N	46·6 W	SHA–LUB
12	—	—	—	—	SHA–TUC
13A	1964 Nov. 30	12:27:39	6·8 N	94·8 E	MNN–FLO
13B	—	—	—	—	FLO–SHA
14	1965 July 5	08:31:58	52·8 N	34·2 W	OGD–OXF
15A	1965 June 2	23:40:24	15·9 N	46·6 W	OGD–AAM
15B	—	—	—	—	AAM–MDS

Downloaded from https://academic.oup.com/gji/article/36/3/515/585195 by guest on 21 August 2022

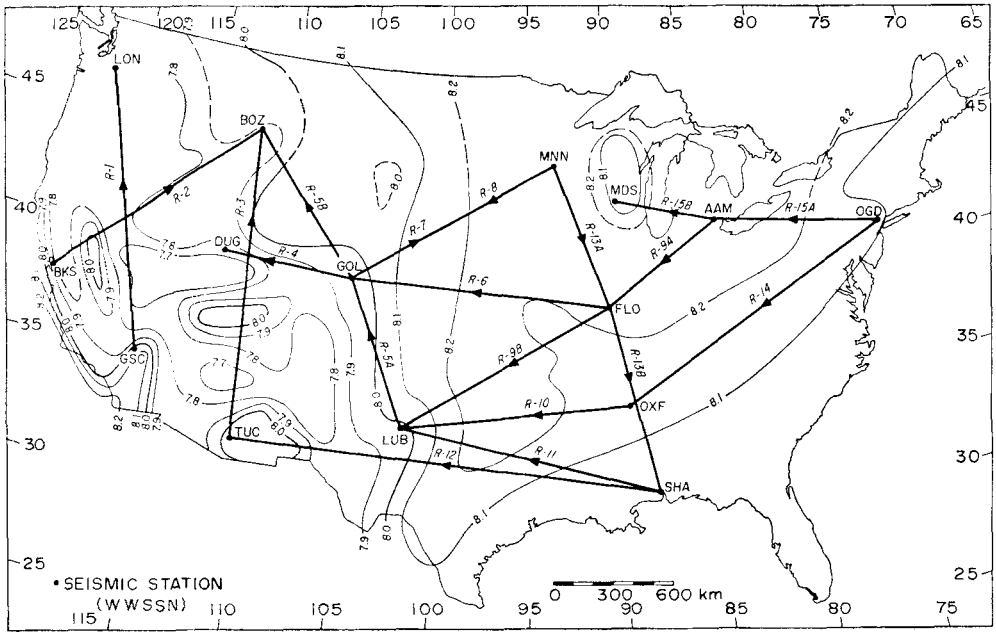

FIG. 1. Location of surface wave profiles in relation to P_n velocity in the continental United States (after Herrin & Taggart 1962).

The event-paths and the station pairs we have used are shown in Fig. 1. The P_n distributions of Herrin & Taggart (1962), with modifications introduced by Archambeau, Flinn & Lambert (1969), are also shown. The events used in our analysis are listed in Table 1.

To obtain phase velocities for each path, the seismograms and the instrument responses of each station have been digitized at a fixed interval of 2 s, an interval sufficiently short to avoid aliasing problems, since negligible signal is recorded on the analogue records at periods shorter than 2 s. We have applied the technique of Pilant & Knopoff (1964) and Knopoff *et al.* (1966) for band-pass, group-arrival-centred, digital filtering of detrended, digitized seismograms to minimize the interference effects of multipath transmission. This procedure significantly improves the signal-to-noise ratio for complex records and allows us to determine the phase reliably for fundamental mode Rayleigh waves over a much broader band of periods than could otherwise have been obtained. In some cases, we have used as many as 20 pass-bands of varying width to determine phases of fundamental mode Rayleigh waves over the period range of 20–300 s. The numerical window centred at the group arrival time was in the form of a half cycle of a sine function. Fourier analysis of each of the filtered seismograms gives the phases in the frequency band of the numerical filters.

Satô (1955, 1956) first applied Fourier analysis to a seismogram to determine the phase velocity of seismic surface waves from a wave train which has travelled a known distance from the epicentre. For two stations on the same great-circle and recording the same event, the phase velocity at a given period T is given by

$$C(T) = \frac{\Delta_2 - \Delta_1}{T\{N + (\phi_2 - \phi_1)\}}$$

where $\Delta_2 - \Delta_1$ is the station separation and where $\phi_2 - \phi_1$ is the difference in the phase shifts (in circles) between the two recordings relative to absolute time, taking into

Downloaded from https://academic.oup.com/gji/article/36/3/515/585195 by guest on 21 August 2022

account instrumental phase shifts. N is an arbitrary integer; each value of N generates a member of a family of phase velocity curves consistent with the data. We have applied the above formula to our observations; the usual technique of selecting N is to find the particular value that gives reasonable values of phase velocity at the longest periods, and to assume the phase velocity curves change smoothly with period.

3. Processing errors

In order to estimate errors in phase velocities introduced by digital processing, we analysed a time series which simulates a noise-free, dispersed long-period seismogram, well defined in both the frequency and time domains. The time series was analysed by the identical operations as were applied to the real seismograms. The results suggested that the pass-bands of the digital filter transmit energy in the period range of 100–200 s with a maximum phase distortion of $\pm 0{\cdot}0012$ circle. In the range of 30–100 s, the pass-bands are characterized by virtually zero phase shifts. For the above two period ranges, the windowing operations gave a maximum phase distortion of $\pm 0{\cdot}0175$ and $\pm 0{\cdot}010$ circle, respectively.

The uncertainty in phase velocity dc is related to the uncertainty in phase $d\phi$ by $dc = (Tc^2/\Delta)d\phi$, where T is the period, c the phase velocity and Δ the distance between the stations. For $\Delta = 800$ km and $c = 4{\cdot}0\,\mathrm{km\,s^{-1}}$ at $T = 100$ s, which are representative figures for this study, a value of $d\phi = 0{\cdot}02$ circle gives rise to an uncertainty of $0{\cdot}04\,\mathrm{km\,s^{-1}}$ in the phase velocity. From this estimate, it may be noted that the errors due to the data processing have contributed an uncertainty of not more than ± 1 per cent at their maximum.

In a heterogeneous earth, the least-time path may not coincide with the least-distance path. This is an important source of error and can be estimated by tripartite observations (Knopoff *et al.* 1966, 1967). This approach however, was not used here since a deviation of the ray from great circle produces erratic fluctuations in the phase velocities which are easily observed (Knopoff *et al.* 1966). We have not encountered any unusual oscillations in the curves to be presented below.

4. Regional phase velocities

Knopoff (1972) compared and classified Rayleigh wave phase velocities for different types of continental regions around the world. The regionalized phase velocities shown below for the western, southcentral and northcentral United States correspond to the rift, young aseismic shields and older aseismic shields respectively in Knopoff's classification.

The characteristics of the Rayleigh wave phase velocities obtained by the method of Section 2 for the different parts of the United States are as follows.

4.1 *Western United States*

This part of the continent was sampled by paths R-1, R-2, R-3, R-4 and R-5B (Fig. 2). Each of the five paths covers, in part, three or more of the Cordilleran geological provinces. Approximately 60 per cent of R-1 lies in the Basin–Range province, and the remainder in the northern plateau. About 40 per cent of R-3 lies in the Colorado plateau and about 50 per cent of R-4 samples the Rocky Mountains. R-2 and R-5B are also mixed and each passes through several geological provinces.

The Rayleigh wave phase velocities obtained for this area are given in Fig. 3. Typical values obtained for the northcentral (R-6) and southcentral (R-11) United States are also shown for comparison. The longest periods for which we have obtained phase velocities are 227 s on R-1, 125 s on R-2, 167 s on R-3, 250 s on R-4 and 132 s on R-5B.

Downloaded from https://academic.oup.com/gji/article/36/3/515/585195 by guest on 21 August 2022

The phase velocities shown in Fig. 3, along the five paths of the Western United States (R-1, -2, -3, -4, -5B) have a profound similarity to one another. In general, the values in this region increase from about 3·6 km s^{-1} at a period of 25 s to about 4·0 km s^{-1} at 90 s, and then gradually increase to about 4·9 km s^{-1} at 250 s (on path R-4). The span of phase velocities among these five profiles is less than 0·05 km s^{-1} except at short periods. The values on all five paths lie within ± 1 per cent of each other in the period range 50–115 s. For periods greater than 115 s, these

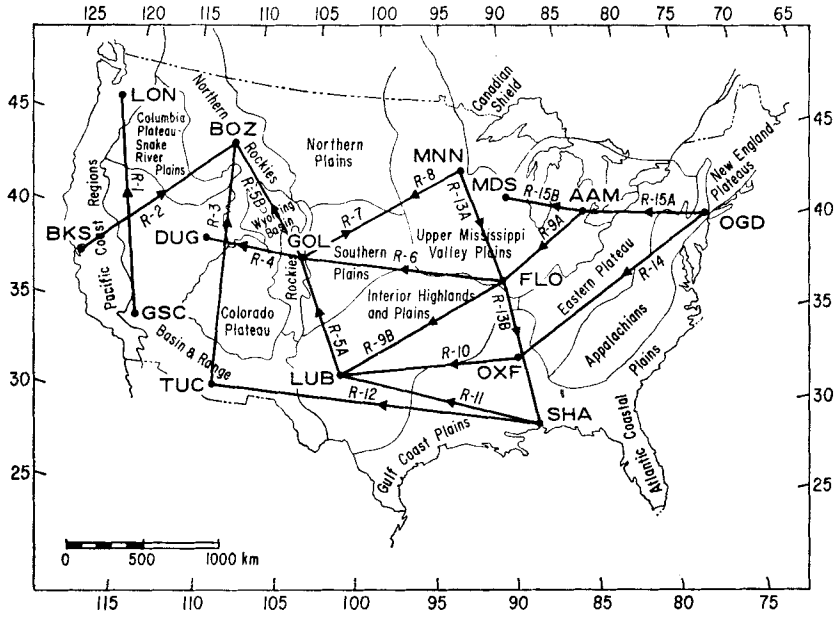

FIG. 2. Location of surface wave profiles with respect to physiographic provinces of the continental United States (after Archambeau *et al.* 1969).

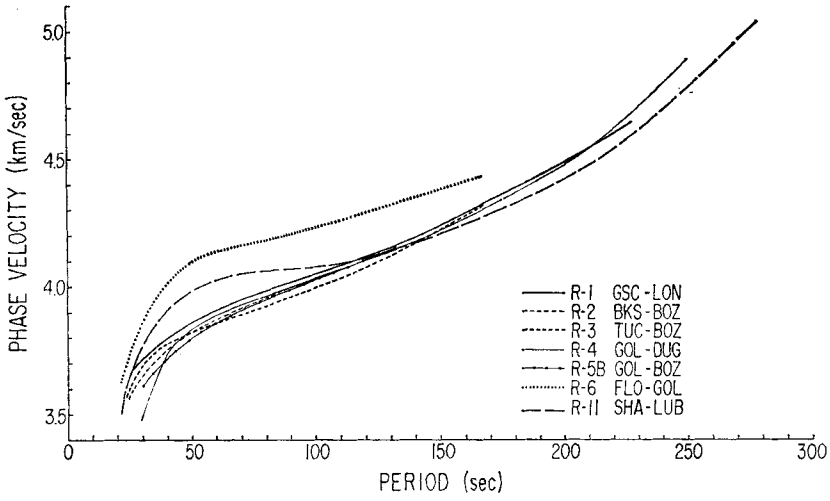

FIG. 3. Rayleigh wave phase velocities for the western United States. Phase velocities for paths R-6 (north-central) and R-11 (south-central) are shown for comparison.

Downloaded from https://academic.oup.com/gji/article/36/3/515/585195 by guest on 21 August 2022

differences are even smaller and can be considered negligible for practical purposes. At periods of 50 s or less, the values on R-1 and R-3 lie very close to each other while those for R-4 are lower by 0·1 to 0·15 km s^{-1} than the others at 30 s.

At short periods we expect variations among the phase velocity curves in the same broad region due to differences in crustal structure. The *S*-wave velocity at the top of the mantle has its maximum influence on Rayleigh waves at periods from 30 to 40 s. This has been checked by computing the appropriate partial derivatives. However, at these periods, the effects of the properties of the crust are not negligible. We believe the low phase velocity of R-4 relative to R-1 and R-3, below 40 s, is related to crustal differences among the paths. The refraction results (Healy & Warren 1969) in the neighbourhood of R-4 suggest a crustal thickening by 7 km compared to that along R-1. This is sufficient to account for the differences we observe. Similarly the differences between the phase velocity on R-1 (GSC–LON) and R-5B which lies within the Colorado plateau are mainly due to differences in crustal structure. Thus, we conclude that, except for differences due to variations in crustal properties, the Rayleigh wave phase velocities in the Western United States, for those paths we have sampled, are uniform to within 1 per cent or less. This observation holds despite the variety of geological provinces sampled by our profiles.

It is useful to give a weak justification for calling this part of the United States a rift zone; elsewhere it has been shown that the phase velocity profile TUC–BOZ(R-3) is virtually indistinguishable from phase velocities measured over the path Addis-Ababa to Nairobi in the East African rift zone (Knopoff & Schlue 1972).

Over the complete range of periods, the phase velocities for the profiles in the Western United States are significantly less than those in the central part (R-6). For periods less than 110 s the phase velocities in the west are less than those on the South-Central profile chosen for comparison (R-11). Above about 140 s, there is a mild cross-over between the profiles in these latter two regions; at periods of the order of 225 s, the south-central phase velocity on R-11 is about 7 or 8 per cent less than on the profile R-1.

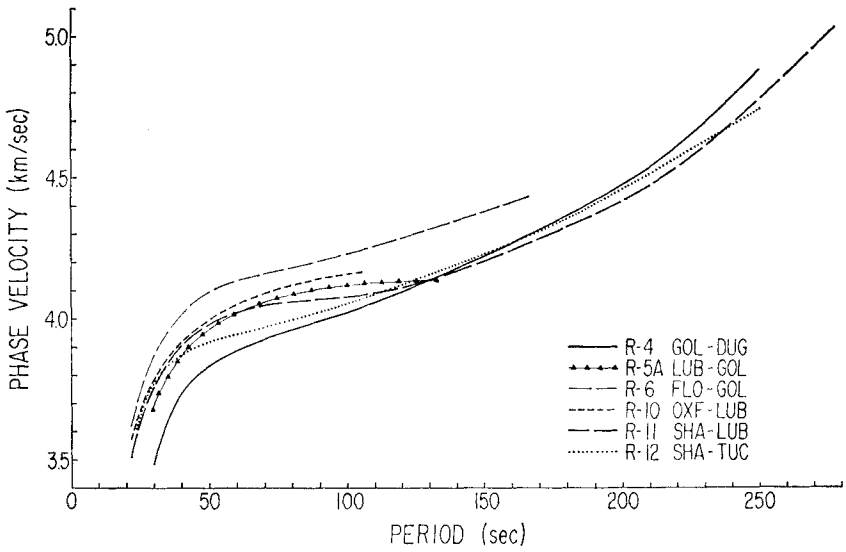

FIG. 4. Rayleigh wave phase velocities for the south-central United States. Phase velocities for paths R-4 (western) and R-6 (north-central) are shown for comparison. Path R-12 is in both the western and south-central regions.

Downloaded from https://academic.oup.com/gji/article/36/3/515/585195 by guest on 21 August 2022

4.2 *South-Central United States*

In Fig. 4 we present the phase velocity curves for the three profiles which lie within the zone of younger shield rocks. These are profiles R-5A, -10, -11. The profile R-12 (SHA–TUC) crosses several provinces; it has part of its path in the younger shields. The values of phase velocity on R-4 and R-6, which are typical of the other structural areas, namely the Western Basin and the North-Central regions respectively, are also shown for comparison. On R-11 and R-12, long-period values up to 277 s and 250 s, respectively, could be obtained, while long-period values are limited to 100 s on R-5A on 130 s on R-10.

The scatter among the three curves for the young shields is small. The phase velocities on R-5A, R-10 and R-11 lie within 1 per cent of each other up to 70 s, and above this period the values of R-11 converge towards those of R-12. In the period range 110–250 s, the phase velocities on these two paths are within 1 per cent of each other. The differences between the curves for the south-central region and the other two regions are significant.

The path R-12, SHA–TUC (see Fig. 1), is the longest of all the paths studied. It covers about 30 per cent of the Gulf Coast, 30 per cent of the central stable region, and 40 per cent of the Basin–Range provinces. This phase velocity curve is intermediate to the rift and young shield curves. The mixed character of this path is displayed by the phase velocities between 50 and 100 s. In this period range, the values are consistently lower by 0·04 km s^{-1} at 250 s. Whether this difference at long periods may be caused by digital processing or not is discussed below.

4.3 *North and East Central United States*

In Fig. 5 we have given our results for the nine paths which lie in the older shield area of the north-central U.S. They differ significantly from the extraordinarily low values of the rift zone, here represented again by R-4 (GOL–DUG) for reference, and are significantly higher than the representative curve for the younger shields,

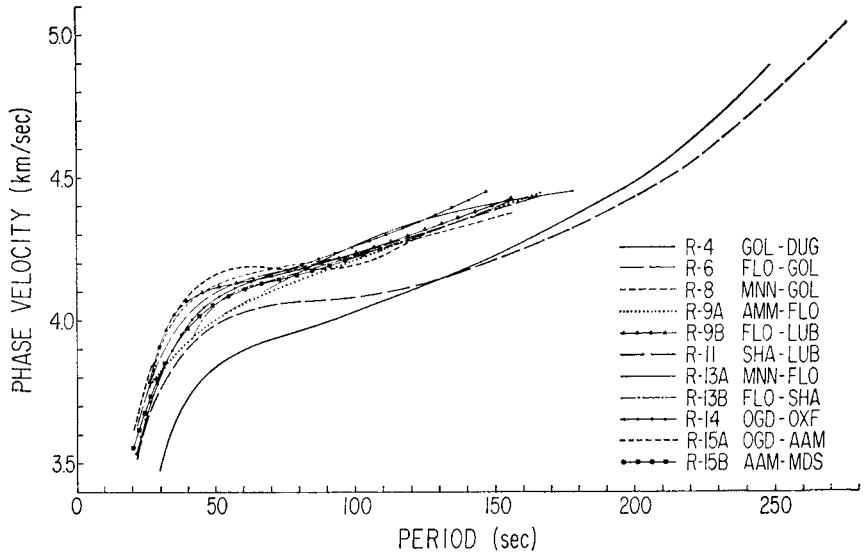

FIG. 5. Rayleigh wave phase velocities for the north-central United States. Phase velocities for paths R-4 (western) and R-11 (south-central) are shown for comparison.

Downloaded from https://academic.oup.com/gji/article/36/3/515/585195 by guest on 21 August 2022

R-11 (SHA–LUB). It should be noted that the curves grouped in this figure were obtained over a relatively larger area compared with the other two areas discussed above.

The phase velocities for the older shield are characteristically high over the entire period range. There are some variations among the nine curves, but the span of differences is less than 0·08 km s^{-1}, except at periods of the order of 50 s where, as in the previous cases, the larger differences may be accounted for in terms of variations in crustal properties.

The phase velocities in this region show significant variation in the period range 30–70 s; the highest values are found on R-15A which is immediately south of the Canadian shield. The lowest values are represented by R-9A which is 50 per cent in the Illinois Basin and 50 per cent in the provinces of the Wisconsin arch and Cincinnati dome. The maximum difference is 0·16 km s^{-1} obtained at 50 s. The values on all other paths fall between the two curves. Above 70 s all the curves lie within about 1 per cent of each other.

It is useful to compare our results with those obtained earlier for the older shield areas. The well-known result of Brune & Dorman (1963) for the Canadian Shield and our profiles for the adjoining regions to the south and west are remarkably consistent. In Fig. 6 we have shown the Canadian Shield results of Brune and Dorman, as well as those of Dorman & Ewing (1962), for the New York–Pennsylvania region, for their limited period range, in comparison with our observations for FLO–GOL (R-6) and OGD-OXF (R-14). The curves are similar except at periods below 50 s. This is probably due to variations of properties of the crust and the topmost mantle in those regions. The shield values have systematically higher phase velocities than the 'standard' curves for the younger shields (R-11) and the rift zone (R-4) which are shown for comparison. Phase velocities inferred from free oscillations (Derr 1969) are not particularly consistent with those for any of the regions; this is consistent with the notion that the free oscillations represent global averages of a most complicated variety, over many different structural types, including oceans.

At this stage of our work, we see no reason to enlarge the number of areas in the classification of the continent beyond the three presented here. The differences among the three groups of curves, are significant.

5. Method of inversion of phase velocity data

5.1 *Sphericity corrections*

The success of the inverse problem depends crucially on our ability to solve the forward problem. The most tractable form of the forward problem involves the

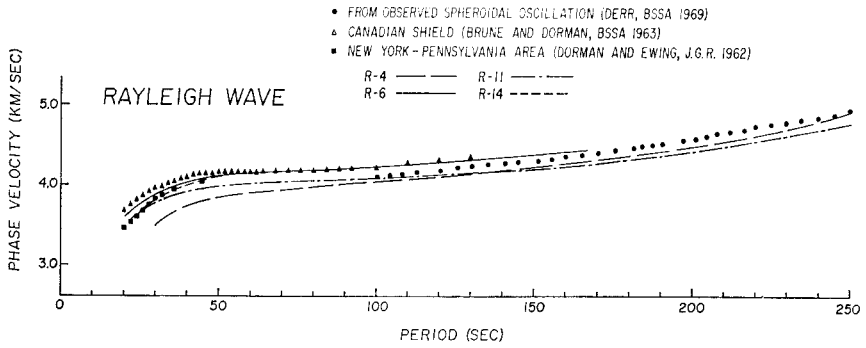

FIG. 6. Comparison of representative phase velocity profiles from this study with Canadian Shield and Pennsylvania results and with free oscillation results.

Downloaded from https://academic.oup.com/gji/article/36/3/515/585195 by guest on 21 August 2022

solution to the problem of the calculation of Rayleigh wave phase velocities for a plane layered earth. Matrix methods for this problem have been designed so that computations can be made with very high speed (Schwab & Knopoff 1970; Schwab 1970).

The phase velocities are measured on an almost spherical earth and thus need to be reduced for curvature effects. Bolt & Dorman (1961) compared phase velocities computed for spherical, gravitating standard earth models with those for the same flat layered earth structures. They have suggested an empirical formula for the Rayleigh wave sphericity corrections.

$$c_s = c_f(1+0{\cdot}00016T), \tag{3}$$

where c_s is the phase velocity at period T (sec) for a gravitating heterogeneous sphere and c_f is the corresponding value for a plane layered earth without gravity. They claim that (3) is valid to within ± 1 per cent of the true values for $100 < T < 300$ s. We used (3) to correct our data.

5.2 *The Hedgehog method*

Keilis-Borok & Yanovskaya (1967) and Press (1968, 1969) proposed that routine multi-model searches be undertaken for the inversion of a given set of earth data. In this method the Earth is represented in the usual way by a set of physical quantities, such as the P- and S-wave velocities, density, and Q-values, whose magnitudes vary with depth. Since we cannot represent the variations of a physical quantity over a certain depth range by a continuous function of adjustable coefficients, if discontinuities in the physical quantities occur, layer representation is perhaps the most appropriate and convenient alternative. The disadvantage of introducing many layers, with several physical quantities to be specified in each layer, is that we increase the number of parameters significantly over that for an algebraic function of relatively low order. If we wish to describe a distribution in the Earth with finer and finer detail, we introduce more parameters by taking finer and finer layers. However, first-order discontinuities are easily introduced by placing them at layer boundaries; the boundary conditions are not violated by this process.

We can imagine the solutions to be points in a multi-dimensional parameter space. A discrete set of models is found at the intersections of a grid, usually of equal dimensions along each of the co-ordinate (parameter) axes. We explore this space and test each model. If there are m variable parameters, each of which is intended to take t values, the total number of different models generated would be t^m. Since this number is usually extraordinarily large, it is necessary to restrict the method of search to make the exploration practical. Each parameter is specified to lie within certain upper and lower bounds; these bounds are obtained from available geophysical information, namely from equations of state concerning the range of values the parameters can have.

The Hedgehog procedure of Keilis-Borok & Knopoff, improves the method of search significantly. At the start, the parameters are given a set of initial values; the corresponding phase velocities are computed and compared with the observations, the latter appropriately reduced for sphericity. If the comparison passes certain acceptance criteria, the search then continues for other solutions in the neighbourhood of the accepted solution. Each neighbourhood of an acceptable solution is then explored in turn without retesting those solutions explored earlier, until the entire singly-connected solution space of acceptability has been covered. This approach provides a large number of successful solutions in a small number of trials, compared with Monte Carlo methods.

The acceptability criteria operate as follows: the phase velocity corresponding to the longest observed period is first computed and compared with the observed

Downloaded from https://academic.oup.com/gji/article/36/3/515/585195 by guest on 21 August 2022

value. If the difference passes through a prescribed tolerance limit, it proceeds to compute and test for the next shorter period and so on. If the test fails at any individual period the model is rejected and a new model is generated in the neighbourhood of the above and tested similarly. However, if the test is successful at all the individual observed periods, the rms difference between computed and observed values is computed and compared with a preset value. This represents an additional acceptance or rejection criterion for the model.

6. Results of the inversions

The implications of the similarity among the five phase velocity profiles in the western U.S. are evidently that the parts of the structure space, which correspond to acceptable solutions, will have strong overlap in the five cases. In the inversion, we have chosen three of the profiles (R-1, R-2, R-4) to see if we could detect any features which do not overlap in the space of acceptable structures and therefore would correspond to detectable gradients in properties across the region. But at the lowest level of the inference from Fig. 3, we conclude that there is a large similarity of structure across the entire region spanned by the five profiles, to depths of the order of 350 km or more. We have chosen R-11 (SHA–LUB), for inversion of phase velocities for the south-central region since it has phase velocity values extending to the longest periods we have measured in this region. We have chosen curve R-6 (FLO–GOL) for inversion of the north-central region. The phase velocities along the five paths chosen for inversion, three from the west and one each from the north-central and south-central regions, are given in Table 2.

In the inversion we introduced three layers between the Moho and the velocity jump corresponding to the phase transformation at a depth of 400–450 km. These three layers are called the lid to the low-velocity channel (LID), the low-velocity channel or zone (LVZ) and the sub-channel (SUB). This nomenclature is applied whether a LVZ is present or not; the second layer is called the LVZ even though the velocity in this zone may be higher than that of the 'lid' (or sub-Moho). By the same token, the layer immediately below the Moho is called the lid whether the channel (the second mantle layer) is indeed an LVZ or not. As noted above, the use of a discrete layered structure for the upper mantle does not imply a commitment on our part to the presence of sharp discontinuities in properties; we cannot resolve fine structure or continuous variations in properties.

Five parameters, namely the S-wave velocities in the three layers, β_{LID}, β_{LVZ}, β_{SUB} and the thicknesses of the lid, h_{LID}, and channel, h_{LVZ}, were allowed to vary simultaneously; thus each model is located in a five-dimensional parameter space. The parameters of the crust were fixed for each region and adjusted to the results of crustal explosion studies. We have had reference mainly to the work of Healy & Warren (1969) but we have also noted the work of Lehmann (1964), Dowling & Nuttli (1964), Green & Hales (1968), Archambeau *et al.* (1969), Helmberger & Wiggins (1971), and Iyer *et al.* (1969). The values of S-wave velocities for the crust were taken from Anderson & Harkrider (1968).

Similarly, the first phase transformation was fixed at 400 km for the rift regions and at 450 km for the others. The parameters below this depth were held fixed and the velocities below these levels were taken from Archambeau *et al.* (1969), Iyer *et al.* (1969) and Anderson & Harkrider (1968).

After fixing the discontinuities and velocities, the densities were set at appropriate depths by using Birch's (1961) relation. P-wave velocities and densities in the three layers between the Moho and the phase transformation were fixed in the sense that, irrespective of layer thicknesses, the same values for these two parameters were retained from model to model. In an independent Hedgehog exploration not reported

Downloaded from https://academic.oup.com/gji/article/36/3/515/585195 by guest on 21 August 2022

Table 2

Observed phase velocities (km s^{-1}) for fundamental mode Rayleigh waves

Period (s)	R-1 GSC–LON	R-3 TUC–BOZ	R-4 GOL–DUG	R-6 FLO–GOL	R-11 SHA–LUB
277·8					5·04
250·0					4·78
227·3					4·59
208·3	4·64				4·47
178·6	4·45		4·70		4·32
156·3	4·33	4·32	4·43		4·23
147·1	4·29	4·26	4·36	4·44	4·20
131·5	4·19	4·17	4·25	4·37	4·16
125·0	4·15	4·12	4·21	4·34	4·14
113·6	4·11	4·07	4·14	4·29	4·11
100·0	4·06	4·01	4·07	4·27	4·08
86·2	4·02	3·96	4·01	4·22	4·07
75·7	3·98	3·92	3·97	4·18	4·06
62·5	3·92	3·87	3·92	4·15	4·04
50·0	3·86	3·83	3·86	4·11	3·98
39·7	3·81	3·78	3·76	4·03	3·90
34·2	3·76	3·73	3·66	3·96	3·84
28·7	3·71	3·68	3·48	3·86	3·74
26·0	3·68	3·63		3·79	3·67
23·6		3·58		3·72	3·59
21·7				3·66	3·51
20·8				3·62	

Table 3

Crust–Upper Mantle structure for the inversion of dispersion on path R-1

Depth (km)	Thickness (km)	β (km s^{-1})	α (km s^{-1})	ρ (g cm^{-3})
0	3	2·0	4·0	2·2
3	15	3·52	6·1	2·77
18	20	3·76	6·68	2·96
38	h_{LID}	β_{LID}	7·84	3·34
$38+h_{LID}$	h_{LVZ}	β_{LVZ}	8·10	3·42
$38+h_{LID}+h_{LVZ}$	$362-h_{LID}-h_{LVZ}$	β_{SUB}	8·57	3·58
400	250	5·2	9·76	3·97
650	410	6·2	11·15	4·43
1060	240	6·48	11·78	4·63
1300	∞	6·62	12·02	4·71

Table 4

Crust–Upper Mantle structure for the inversion of dispersion on path R-3

Depth (km)	Thickness (km)	β (km s^{-1})	α (km s^{-1})	ρ (g cm^{-3})
0	2	2·0	4·0	2·2
2	25	3·65	6·2	2·80
27	18	3·83	6·73	2·98
45	h_{LID}	β_{LID}	7·85	3·34
$45+h_{LID}$	h_{LVZ}	β_{LVZ}	7·83	3·34
$45+h_{LID}+h_{LVZ}$	$355-h_{LID}-h_{LVZ}$	β_{SUB}	8·44	3·54
400	250	5·2	9·76	3·97
650	410	6·2	11·15	4·43
1060	240	6·48	11·78	4·63
1300	∞	6·62	12·02	4·71

Downloaded from https://academic.oup.com/gji/article/36/3/515/585195 by guest on 21 August 2022

Table 5

Crust–Upper Mantle structure for the inversion of dispersion path R-4

Depth (km)	Thickness (km)	β (km s^{-1})	α (km s^{-1})	ρ (g cm^{-3})
0	1·5	2·0	4·0	2·2
1·5	1·5	2·85	5·0	2·41
3	10	3·43	5·6	2·61
13	17	3·45	5·65	2·62
30	18	3·69	6·7	2·97
48	h_{LID}	β_{LID}	7·9	3·36
$48+h_{LID}$	h_{LVZ}	β_{LVZ}	8·07	3·41
$48+h_{LID}+h_{LVZ}$	$352-h_{LID}-h_{LVZ}$	β_{SUB}	8·5	3·56
400	258	5·2	9·76	3·97
658	410	6·2	11·15	4·43
1068	240	6·48	11·78	4·63
1308	∞	6·62	12·02	4·71

Table 6

Crust–Upper mantle structure for the inversion of dispersion on path R-6

Depth (km)	Thickness (km)	β (km s^{-1})	α (km s^{-1})	ρ (g cm^{-3})
0	1	2·83	4·9	2·38
1	10	3·45	5·9	2·70
11	18	3·78	6·15	2·79
29	16	3·95	6·7	2·57
45	h_{LID}	β_{LID}	8·17	3·45
$45+h_{LID}$	h_{LVZ}	β_{LVZ}	8·4	3·52
$45+h_{LID}+h_{LVZ}$	$405-h_{LID}-h_{LVZ}$	β_{SUB}	8·8	3·65
450	200	5·3	9·8	3·98
650	400	6·2	11·15	4·43
1050	240	6·48	11·78	4·62
1290	∞	6·62	12·02	4·71

Table 7

Crust–Upper Mantle structure for the inversion of dispersion on path R-11

Depth (km)	Thickness (km)	β (km s^{-1})	α (km s^{-1})	ρ (g cm^{-3})
0	10	3·49	6·05	2·75
10	20	3·67	6·35	2·85
30	20	3·85	7·05	3·08
50	h_{LID}	β_{LID}	8·17	3·45
$50+h_{LID}$	h_{LVZ}	β_{LVZ}	8·35	3·54
$50+h_{LID}+h_{LVZ}$	$400-h_{LID}-h_{LVZ}$	β_{SUB}	8·8	3·65
400	200	5·3	9·8	3·98
650	400	6·2	11·15	4·43
1050	240	6·48	11·78	4·63
1290	∞	6·62	12·02	4·71

Downloaded from https://academic.oup.com/gji/article/36/3/515/585195 by guest on 21 August 2022

in this paper, the mantle densities have been taken to be parameters in the search as well as the S-wave velocities. We find no significant differences from the results reported here; only the edge of the solution space is shifted slightly from the description below. The velocity and density models for the crust and upper mantle, used in the inversion for each of the five profiles, are given in Tables 3–7. The parameters fixed in the inversion are listed; the five parameters in the Hedgehog exploration are indicated.

One possibility in the inversion which was available to us was to use the known values of P_n velocities as determinants of the S-wave velocity in the lid for those regions where S_n data are not directly available, and to use S_n data where available, to place bounds on lid velocities (Huestis, Molnar & Oliver 1973). We have preferred not to make *a priori* judgments concerning this parameter and have instead allowed it to vary over a rather broad range, as one of the five parameters in the Hedgehog system. After the catalogue of acceptable solutions has been constructed, then we can reject certain solutions as being inconsistent with observations of P_n and S_n if we wish.

The estimated uncertainty in the observed phase velocities, as mentioned above, is of the order of ± 1 per cent, especially for periods greater than 200 s. This uncertainty is $\pm 0{\cdot}05\,\mathrm{km\,s^{-1}}$ at a period of 250 s. In the inversion, if the difference between computed and observed phase velocities exceeded the limit of $\pm 0{\cdot}05\,\mathrm{km\,s^{-1}}$ at any individual period, the model was rejected. Models which passed these tests, were further tested to determine whether the rms deviation σ was appropriately small. All models with $\sigma \leqslant 0{\cdot}03\,\mathrm{km\,s^{-1}}$ were finally accepted. With these constraints, the results of the inversion in the five-dimensional representation of model space are shown in Figs 7, 8 and 9.

In Figs 7, 8 and 9, the abscissae and ordinates of the inner, small rectangles represent the lid thickness and the LVZ thickness, respectively. The values of these two variables are indicated in the insert rectangle at the left side of each Figure. The rectangular block formed by the array of inner rectangles represents the other three variables. Each block is identified by a different β_{SUB} indicated immediately below the block. The other two co-ordinates of each block give β_{LVZ} and β_{LID} (for a given β_{SUB}).

The search for acceptable rift zone models was conducted within the grid:

$$\beta_{LID} = 4{\cdot}25\ (0{\cdot}1)\ 4{\cdot}95\,\mathrm{km\,s^{-1}},$$
$$\beta_{LVZ} = 4{\cdot}1\ \ (0{\cdot}1)\ 4{\cdot}6\ \ \mathrm{km\,s^{-1}},$$
$$\beta_{SUB} = 4{\cdot}45\ (0{\cdot}15)\ 5{\cdot}05\,\mathrm{km\,s^{-1}},$$
$$h_{LID} = 5\ \ \ (30)\ \ 95\ \mathrm{km},$$
$$h_{LVZ} = 100\ (50)\ 300\ \mathrm{km}.$$

The list above indicates in order the smallest value of the parameters, the grid interval, and the largest value of the parameter of the search. The Hedgehog procedure ensures that not all 4800 lattice points of the 5-dimensional grid are explored; only those in the neighbourhood of 'acceptable' solutions are tested.

The acceptable rift zone models are shown in Fig. 7. No acceptable solutions were obtained with the four combinations $\beta_{LVZ} = 4{\cdot}1\,\mathrm{km\,s^{-1}}$ or $\beta_{LVZ} = 4{\cdot}5\,\mathrm{km\,s^{-1}}$ and $\beta_{SUB} = 4{\cdot}9\,\mathrm{km\,s^{-1}}$ or $\beta_{SUB} = 5{\cdot}05\,\mathrm{km\,s^{-1}}$. Similarly the Hedgehog program searched, unsuccessfully, for solutions with $\beta_{LVZ} = 4{\cdot}6\,\mathrm{km\,s^{-1}}$ and β_{SUB} ranging from 4·45 to $4{\cdot}75\,\mathrm{km\,s^{-1}}$; the program did not explore the other possible solutions outside the parameter sub-space shown in Fig. 7. Nine structures were simultaneously acceptable for both paths R-1 and R-3, of which seven had $h_{LID} = 5\,\mathrm{km}$. These are shown in the figure by stars.

Downloaded from https://academic.oup.com/gji/article/36/3/515/585195 by guest on 21 August 2022

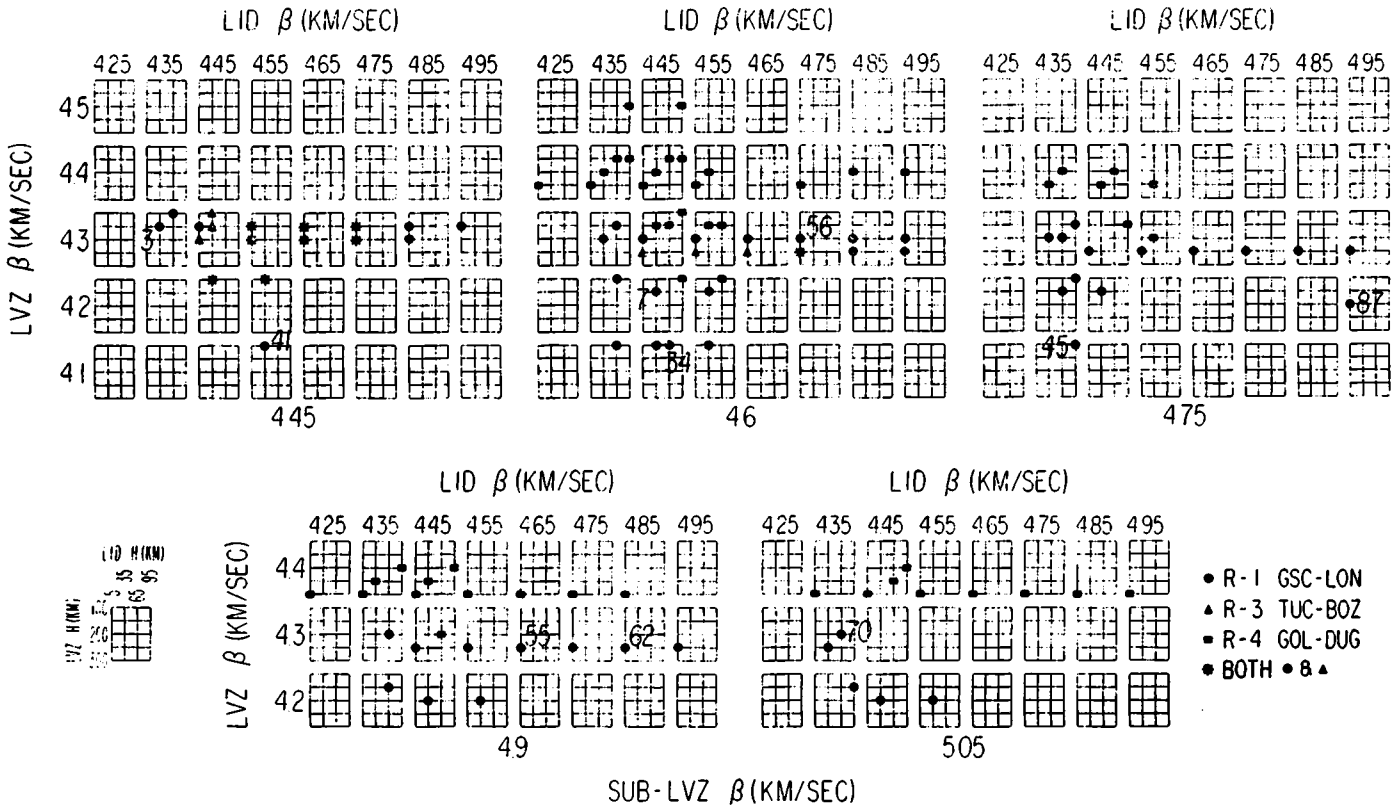

FIG. 7. Five-dimensional model space of acceptable solutions for inversions of three phase velocity profiles in the western United States.

Downloaded from https://academic.oup.com/gji/article/36/3/515/585195 by guest on 21 August 2022

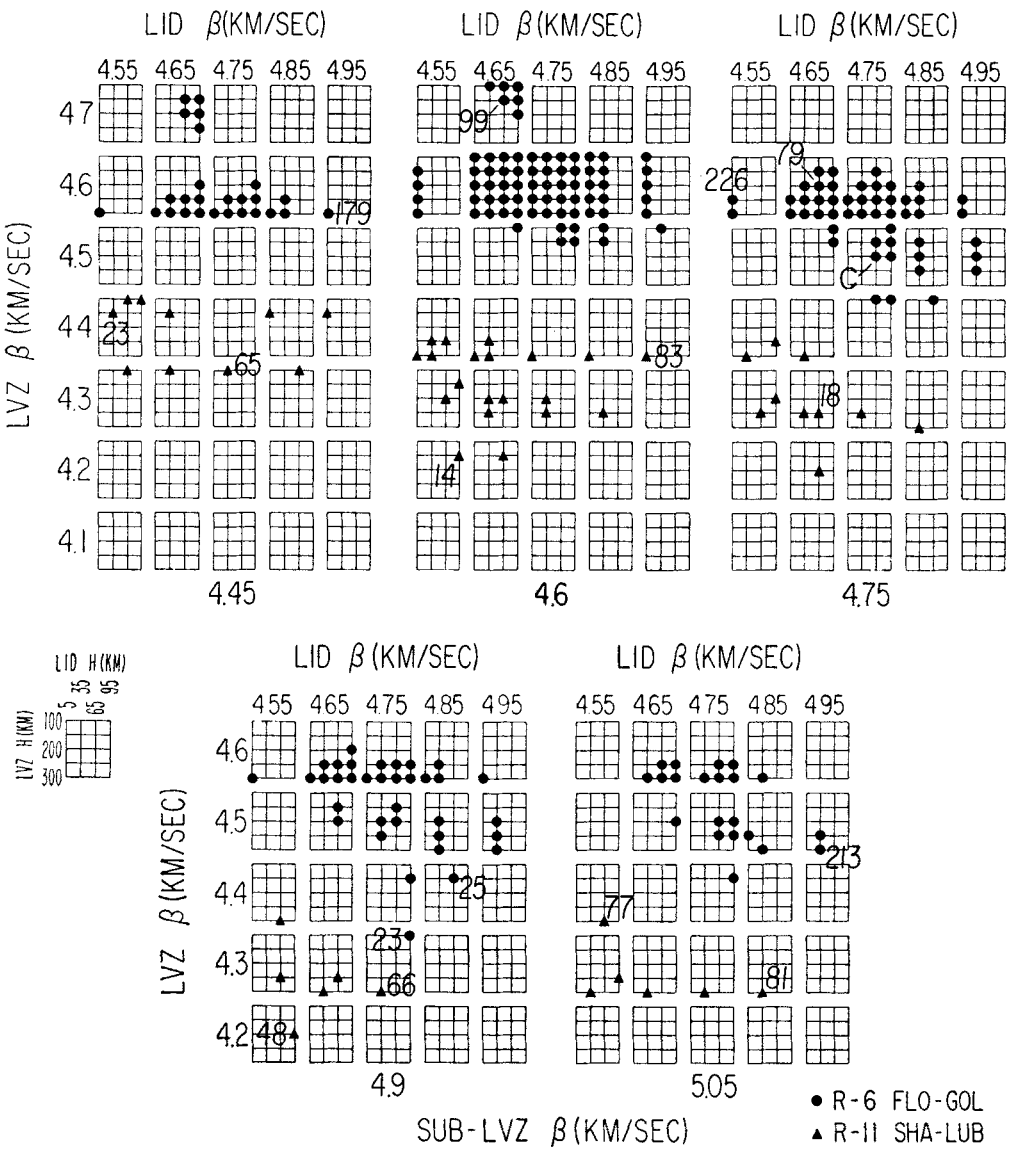

FIG. 8. Five-dimensional model space of acceptable solutions for inversion of phase velocity profiles in north-central (R-6) and south-central (R-11) United States.

On path R-3, no solution was found with β_{SUB} greater than 4·6 km s^{-1}. Similarly we found no solution for R-4 with $\beta_{SUB} = 4{\cdot}45$ km s^{-1}.

All of the models obtained for paths R-1 and R-3 have an LVZ of thickness 100–250 km which is relatively well developed, i.e. which has a strong *S*-wave velocity contrast to the regions above and below. The *S*-wave velocity in the channel ranges from less than 4·1 to 4·3 km s^{-1}. If the lid velocity is as high as 4·55 km s^{-1}, the thickness of the lid cannot be as great as 65 km for any subchannel velocity. For models with lower lid velocities, it becomes difficult to distinguish between a lid and a channel, since their velocities are comparable in some cases. The velocities of the lid and sub-LVZ show variations over a considerable range of values but models with

Downloaded from https://academic.oup.com/gji/article/36/3/515/585195 by guest on 21 August 2022

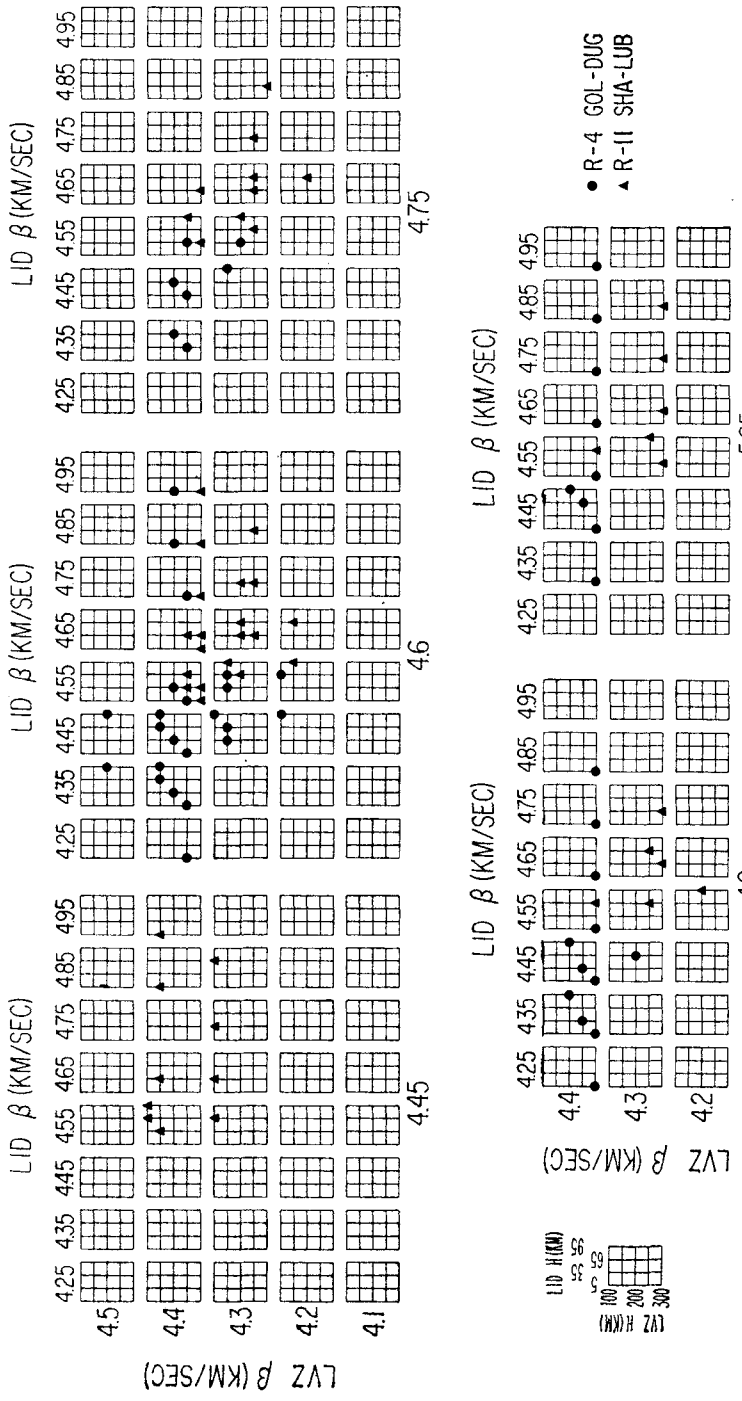

FIG. 9. Comparison of acceptable solutions for inversion of phase velocity profiles in western (R-4) and south-central (R-11) United States.

Downloaded from https://academic.oup.com/gji/article/36/3/515/585195 by guest on 21 August 2022

a fast, thin lid are always associated with a wide LVZ. When $\beta_{LVZ} = 4{\cdot}3\,km\,s^{-1}$, all models with $\beta_{LID} = 4{\cdot}35\,km\,s^{-1}$ have $h_{LID} = 5\,km$.

The models on path R-4 tend to have a shear wave velocity in the channel of $4{\cdot}4\,km\,s^{-1}$, though there are some solutions with β_{LVZ} of 4·2 and $4{\cdot}3\,km\,s^{-1}$. None of the acceptable models on R-4 are also acceptable models for R-1 and R-3. On path R-4 we find that the models have the combination of a relatively thicker lid (35–95 km) and narrower channel (100–200 km) than in the Basin and Range to the west. The models for this path, in general, have a higher average *S*-wave velocity in the upper mantle compared with the structures for R-1 and R-3.

In Fig. 10 we have displayed by conventional velocity cross-sections some of the extreme solutions (identified by numbers in Fig. 6) obtained on path R-3. Structure number 87 is an example of the extreme case of a thin high-velocity lid compensated by a wide channel with a low *S*-wave velocity. Structure number 41 is an example of a lid with a moderate *S*-wave velocity and a pronounced channel represented by two layers; the lower layer occupies the depth interval 180–400 km. Structure number 34 is a case of the combination of a lid of thickness 65 km having a moderately slow *S*-wave velocity and a well-developed channel. An extreme case of the virtual absence of a channel is represented by structure number 3. In this case the *S*-wave velocity is uniformly low, namely about $4{\cdot}3\,km\,s^{-1}$ in both regions

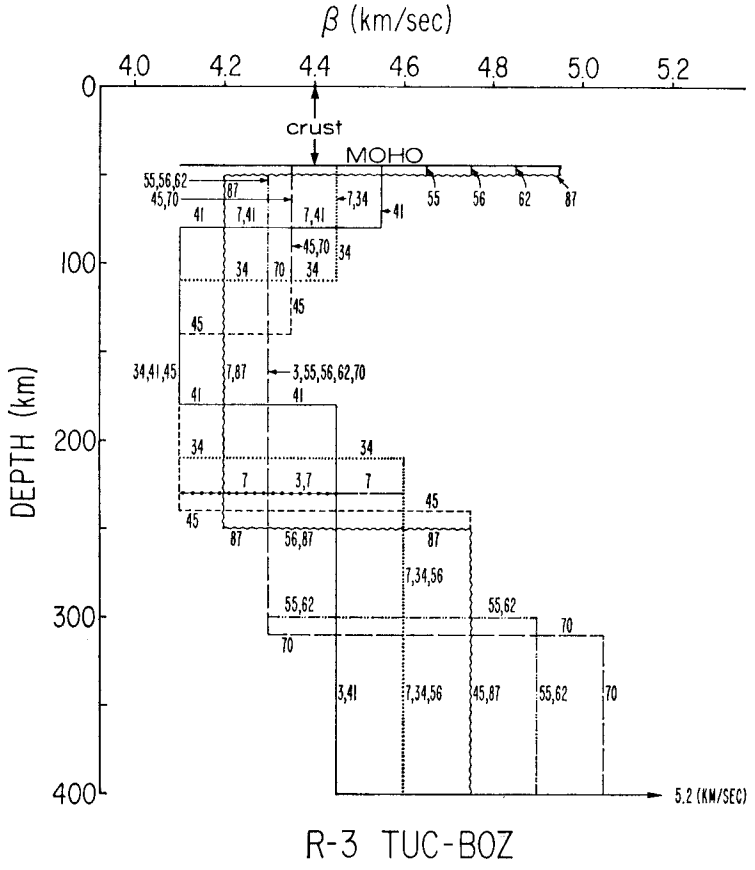

FIG. 10. Shear velocity cross-sections for representative models in the inversion of the phase velocity profile for path R-3, Tucson–Bozeman, western United States. Model numbers correspond to those of Fig. 7.

Downloaded from https://academic.oup.com/gji/article/36/3/515/585195 by guest on 21 August 2022

nominally separated into lid and channel; we may say the lid has zero thickness and the low-velocity channel extends up to the Moho.

The models obtained in the aseismic south-central platform (R-11) and the north-central shield (R-6) regions are shown in Fig. 8. The steps for the variations of velocities and thicknesses in the Hedgehog search were the same as for the earlier example of the rift zone. For both regions we have searched for possible solutions with $\beta_{LID} = 4{\cdot}45\,km\,s^{-1}$ with β_{SUB} varying from 4·45 to $5{\cdot}05\,km\,s^{-1}$. We have searched also for the combination of $\beta_{LVZ} = 4{\cdot}1\,km\,s^{-1}$ with the values of β_{SUB} of 4·9 and $5{\cdot}05\,km\,s^{-1}$. No solutions were found for the above cases. An upper bound of $\beta_{LVZ} = 4{\cdot}7\,km\,s^{-1}$ was set in the search; as noted above, we call this second layer the LVZ even though a channel might not exist.

The solutions for the two regions have pronounced differences. In the southern regions, the solutions consistently indicate the presence of a well-developed LVZ with β in the channel varying from 4·2 to $4{\cdot}4\,km\,s^{-1}$. On the other hand, the shield models tend to cluster with β in the 'channel' of $4{\cdot}6\,km\,s^{-1}$. Thus in the north, we find the presence of a channel of low contrast to the lid above. In some cases we find that the data are satisfied by models without channels. There is nominal scatter among the solutions for the northern shield. Solutions numbers 23 and 99 (solid circles) are examples of the extremes of the scatter.

Overall, significant differences in structure are found between the two regions. It is notable that no solutions are found in common between the solutions for R-6 and R-11. This is perhaps to have been expected since the phase velocity curves differ by more than the allowable uncertainty in measurement of each. As an example of the differences between the two regions we may compare solution number 23 for R-6 with solution number 66 of R-11. Both have the same velocities in each of the three layers. Nevertheless, the shield structure (R-6) has a thick lid and a narrow channel while the young coastal zone (R-11) has a thin lid and a wide channel. The most notable feature about the comparison of the structures for R-6 and R-11 that can be seen from Fig. 7 is the rather obvious 'barrier' of LVZ velocities, forbidden to both profiles and separating both. At the lower subchannel velocities, a channel velocity of $4{\cdot}5\,km\,s^{-1}$ is forbidden to both; the shield area has its lowest channel velocities at $4{\cdot}6\,km\,s^{-1}$ while the younger region has as its highest channel velocities, values of $4{\cdot}4\,km\,s^{-1}$. At higher sub-channel velocities the 'barrier' channel velocity drops slightly, namely the channel velocities found in the northern shield area are as low as $4{\cdot}5\,km\,s^{-1}$ while the highest channel velocities found in the southern areas are $4{\cdot}3\,km\,s^{-1}$.

The velocity-depth cross-sections for some of the extreme solutions for the southern region (R-11) of Fig. 8, are shown in Fig. 11. It is difficult to identify the thickness of the lid to the channel; if we reject models with lid velocities greater than $4{\cdot}75\,km\,s^{-1}$ as inconsistent with observations of S_n velocities (Huestis *et al.* 1973), and if the subchannel has velocities greater than $4{\cdot}6\,km\,s^{-1}$, the least lid thickness is always greater than 5 km and less than 35 km. Unfortunately, our exploration is not fine enough to resolve this point. As before, the lid thickness of 5 km is introduced to avoid a possible blow-up of the computer program for lids of zero thickness. Models including a 5 km lid over a prominent low velocity channel have dispersion curves which are consistent with those of a lid of zero thickness over the same channel to within our accuracy of fit for all periods we have used. In this connection, models such as solution 83 are of interest since, excluding a 5-km veneer of high velocity material, they indicate that the data can be satisfied by assuming that a region with uniform *S*-wave velocity exists to great depth. In this case, the velocity of the uniform upper mantle is the highest allowable for a channel reaching to Moho, i.e. without a lid, and is $4{\cdot}4\,km\,s^{-1}$. With more well-defined high-velocity lids, the channel velocities are correspondingly lower. For example, solution 18 has a lid with $\beta = 4{\cdot}65\,km\,s^{-1}$ and a $4{\cdot}3\,km\,s^{-1}$ channel starting at 115 km below the surface. In cases 14

Downloaded from https://academic.oup.com/gji/article/36/3/515/585195 by guest on 21 August 2022

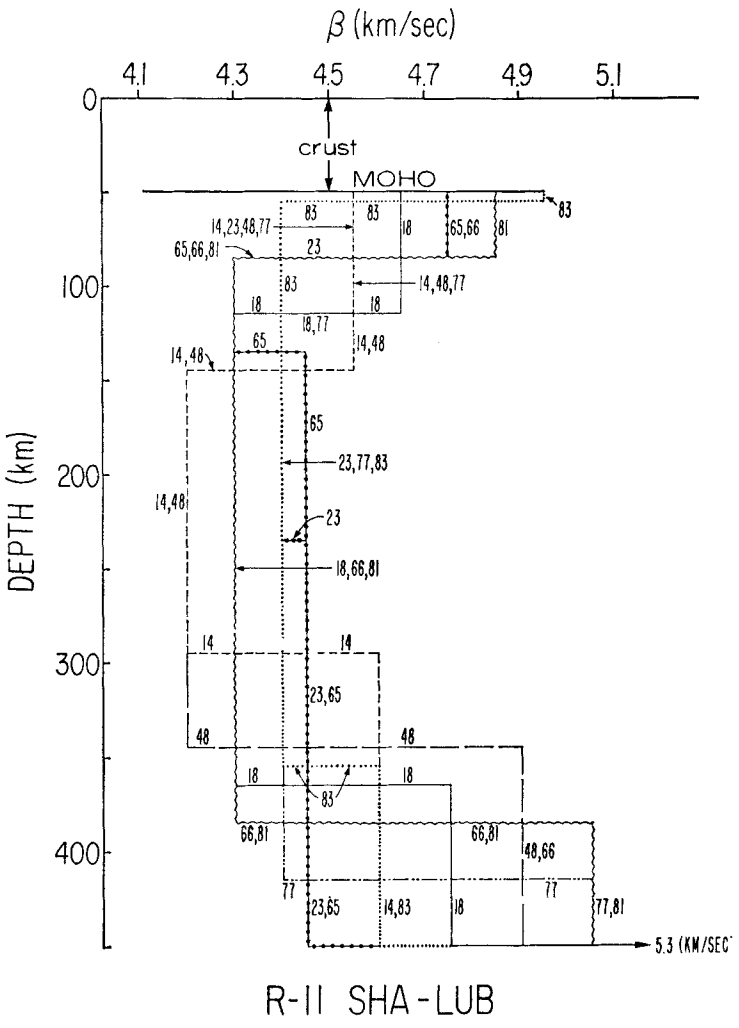

FIG. 11. Shear velocity cross-sections for representative models in the inversion of the phase velocity profile for path R-11, Spring Hill–Lubbock, south-central United States. Model numbers correspond to those of Fig. 8.

and 48 the lid is even thicker and the channel velocity even lower. In general, the other structural solutions are intermediate to those already described.

Similarly, some of the solution cross-sections (for solution numbers see Fig. 8) for the northern shield path R-6, are shown in Fig. 12. Solution numbers 23, 25 and 213 demonstrate the lid-channel coupling; as the lid becomes thicker and slower, the channel becomes narrower and slower. If the lid velocity is close to $4{\cdot}6\,\mathrm{km\,s^{-1}}$, solutions numbered 226, 79, 179, and 99 indicate that an absence of a channel, or a very small positive or negative velocity gradient are consistent with the data.

In Fig. 12 the Canadian shield model (CANSD) of Brune & Dorman (1963) is also shown for comparison with some of our models obtained in this study. CANSD is completely consistent with our class of solutions to the inversion of profile R-6, and would appear to be a member of that class. We have identified one of our acceptable models for path R-6, indicated as C on Fig. 8, which seems to approximate CANSD very closely. Model C is indicated in Fig. 12 for comparison.

Downloaded from https://academic.oup.com/gji/article/36/3/515/585195 by guest on 21 August 2022

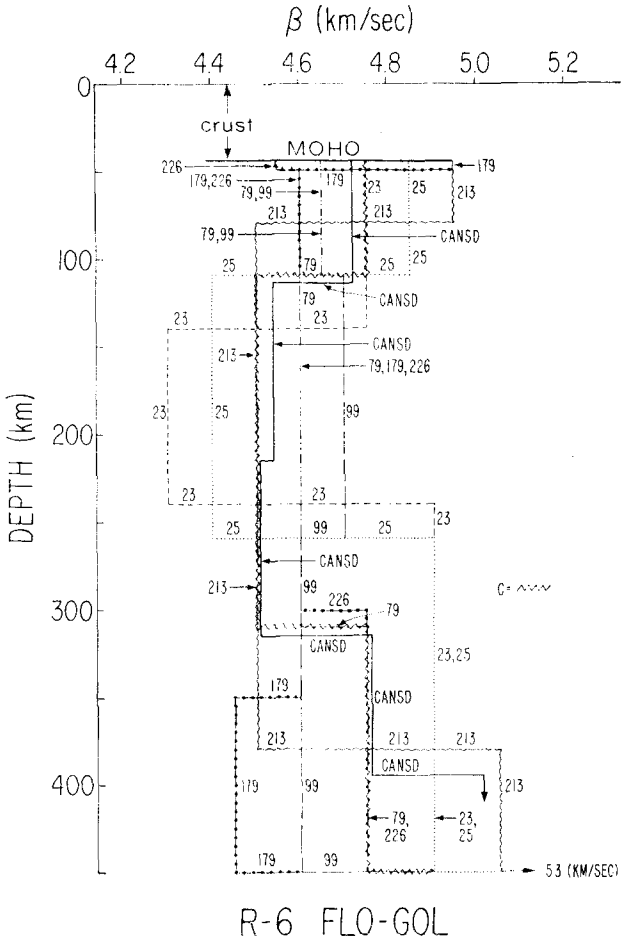

FIG. 12. Shear velocity cross-sections for representative models in the inversion of the phase velocity profile for path R-6, Florissant–Golden, north-central United States. Mode numbers correspond to those of Fig. 8.

The difference between the upper mantle structures for the northern shields (R-6) and the southern stable regions (R-11) are quite well marked. The upper mantle *S*-wave velocities are generally higher throughout the uppermost 250 km for the northern regions. Solutions for both regions can be found without lids (or channels); in these cases, the upper mantle *S*-wave velocity is about 4·4 km s^{-1} for the southern regions while it is about 4·6 km s^{-1} for the northern regions. If more high velocity material is introduced into the topmost upper mantle, a lower channel velocity than the two values above is obtained. Since the P_n (Fig. 1) and S_n (Huestis *et al.* 1973) velocities in the southern stable regions are comparable to those of the northern shields, it seems very likely that the southern regions have a rather pronounced high velocity lid and a well-defined channel with a velocity of 4·3 km s^{-1} or less. No such channel is required for the northern regions.

It is useful to compare the structures of the upper mantle to the west of the Rocky Mountain Front with those immediately to the east of the Front. Both these regions are characterized by the presence of significant amounts of low-velocity material at depths of the order of 100–200 km in the north. These regions are characterized by paths R-4 for the Colorado Plateau (GOL–DUG) and R-5A (LUB-GOL) for the region immediately to the east. Since we have chosen to invert R-11 as the typical

Downloaded from https://academic.oup.com/gji/article/36/3/515/585195 by guest on 21 August 2022

member of the family to which R-5A belongs, we compare the inversions of paths R-4 and R-11. This comparison, which is in fact a fusion of parts of the results already presented in Figs 7 and 8, is shown in Fig. 9. A crude assessment of this figure shows that the two sets of solutions spaces do not overlap. It is appropriate to see what the differences are. Let us assume that the S_n or lid velocity for R-11 is greater than $4{\cdot}6\,\mathrm{km\,s^{-1}}$, which is not inconsistent with the observations of S_n in this region. Let us further reject solutions with lid thicknesses of 5 km, as being artifacts of the method of analysis, for both profiles. Then we find that all of the solutions for R-4 have S_n velocities less than $4{\cdot}6\,\mathrm{km\,s^{-1}}$.

This difference can be illustrated in another way. We find that if the uppermost 300 km of the upper mantle is allowed to be material with S-wave velocity of $4{\cdot}4\,\mathrm{km\,s^{-1}}$, we can obtain a solution for both R-11 and R-4, but this is done at the expense of introducing a sub-channel region with S-wave velocity $4{\cdot}6\,\mathrm{km\,s^{-1}}$ for the Colorado Plateau and a sub-channel with velocity $5{\cdot}05\,\mathrm{km\,s^{-1}}$ for the Gulf Coast. In short the differences between the dispersion curves for profiles R-4 and R-11 (Fig. 3) in the period range 50–70 s are large and require the introduction of significant amounts of high-velocity material under R-11 relative to R-4 somewhere in the uppermost 400–450 km of the mantle. We prefer to place this high velocity material under R-11 in the lid zone, immediately below the Moho, since this corresponds more closely to the refraction observations.

7. Conclusions

We have made measurements of the dispersion of Rayleigh waves to periods occasionally as long as (about) 280 s on 18 profiles in the United States. The accuracy of the measurements is probably of the order of $\pm 0{\cdot}05\,\mathrm{km\,s^{-1}}$ at 250-s period and is better than this value at shorter periods.

The phase velocity curves can be arranged into three groups. The phase velocities on nine profiles in the north-central United States compare closely with published values for the Canadian shield. These phase velocities are the highest we have observed. On three profiles in the south-central area, we have found phase velocities which are significantly lower than the first group. The lowest phase velocities are found on five profiles between the Rocky Mountains and the Sierra Nevada; these latter phase velocities compare closely with those observed for the East African Rift Zone. Each of the phase velocities almost always falls within experimental uncertainty of the other members of its group. One profile (SHA–TUC) lies in two provinces and has phase velocities which are intermediate to the two regions.

The upper mantle structure down to a depth of from 200 to 400 km has been determined by inversion of the dispersion curves. The depth range depends closely on the maximum periods obtained in the dispersion curves. The non-uniqueness in the inversion permits us to draw only certain general conclusions about the structure of the upper mantle in these regions. The upper mantle under the north-central part of the United States is underlain by material with high S-wave velocities, namely with velocities around $4{\cdot}6$ or $4{\cdot}7\,\mathrm{km\,s^{-1}}$ extending to great depths. Our data are fit equally well by structures with very small channels as by structures with zero or small positive gradients, at least to the accuracy of our measurements. Under the south-central part of the United States, if the lid S-wave velocities are as high as $4{\cdot}6\,\mathrm{km\,s^{-1}}$, a marked channel is found below the lid. If the channel starts at a depth of 80 km below the surface, then the channel S-wave velocity can be as low as $4{\cdot}2\,\mathrm{km\,s^{-1}}$. In this region we have no solutions without channels for these relatively high lid velocities.

In the western part of the United States, we have obtained rather low S-wave velocities in the upper mantle extending to the greatest depths of penetration which we are able to obtain with our data. In this region we obtained solutions with velocities such as $4{\cdot}4\,\mathrm{km\,s^{-1}}$ rising up to the Mohorovičić discontinuity. Lower channel

Downloaded from https://academic.oup.com/gji/article/36/3/515/585195 by guest on 21 August 2022

velocities are not atypical. We are unable to resolve the profiles TUC–BOZ and GSC–LON; we see a hint of higher velocities at great depth under the profile GOL–DUG in comparison with the other two profiles we have inverted in this region.

Crudely, the three regions may be compared as follows: under the extension of the Canadian Shield to the south, a mild (or no) LVZ is found in the upper mantle. Under the Gulf States westward to LUB–GOL, a pronounced low-velocity channel can be imagined to occupy part of the northern shield structure, starting at a depth of between 80 and 140 km. In the western states, the lid to the Gulf structure may be imagined to have thinned to almost zero thickness beneath the crust, i.e. the channel introduced in the Gulf structure into the northern shield structure has now been broadened until it virtually extends to the Mohorovičić discontinuity under the western basin states.

These results are well correlated with heat flow observations (Roy *et al.* 1968; Simmons & Roy 1969). The heat flows are least in the north-central regions and greatest in the western basin. The velocities in the LVZ of the Gulf states and the Western regions can only be accounted as being due to partial melting of the upper mantle material (Birch 1969); under the northern shield, no partial melting need be involved.

Acknowledgments

This research was supported in part by Grant GA–18672 of the National Science Foundation and in part by Grant AFOSR–69–1808 of the Air Force Office of Scientific Research.

Institute of Geophysics and Planetary Physics,
University of California, Los Angeles.

References

Anderson, D. L., 1967. Latest information from seismic observations, *The Earth's Mantle*, 355–419, ed. T. F. Gaskell, Academic Press, London and New York.

Anderson, D. L. & Harkrider, D. G., 1968. Universal dispersion tables, II. Variational parameters for amplitudes, phase velocity and group velocity for first four Love modes for an oceanic and a continental Earth model, *Bull. seism. Soc. Am.*, **58**, 1407–1499.

Archambeau, C. B., Flinn, E. A. & Lambert, D. G., 1969. Fine structure of the Upper Mantle, *J. geophys. Res.*, **74**, 5825–5865.

Birch, F., 1969. Density and composition of the Upper Mantle: first approximation as an olivine layer, in *The Earth's Crust and Upper Mantle*, ed. P. J. Hart, *Am. geophys. Union, Monograph* **13**, 18–36.

Birch, F., 1961. The velocity of compressional waves in rocks to 10 kilobars, part 2, *J. geophys. Res.*, **66**, 2199–2224.

Bolt, B. A. & Dorman, J., 1961. Phase and group velocities of Rayleigh waves in a spherical, gravitating Earth, *J. geophys. Res.*, **66**, 2965–2981.

Brune, J. & Dorman, J., 1963. Seismic waves and Earth structure in the Canadian Shield, *Bull. seism. Soc. Am.*, **53**, 167–210.

Derr, J. S., 1969. Free oscillation observations through 1968, *Bull. seism. Soc. Am.*, **59**, 2079–2099.

Dorman, J., 1969. Seismic surface-wave data on the Upper Mantle, in *The Earth's Crust and Upper Mantle*, ed. P. J. Hart, *Am. geophys. Union, Monograph* **13**, 257–265.

Downloaded from https://academic.oup.com/gji/article/36/3/515/585195 by guest on 21 August 2022

Dorman, J. & Ewing, M., 1962. Numerical inversion of seismic surface wave dispersion data on Crust–Mantle structure in the New York–Pennsylvania area, *J. geophys. Res.*, **67,** 5227–5241.

Dowling, J. & Nuttli, O., 1964. Travel time curves for a low-velocity channel in the Upper Mantle, *Bull. seism. Soc. Am.*, **54,** 1981–1996.

Dziewonski, A. M., 1971a. On regional differences in dispersion of Mantle Rayleigh waves, *Geophys. J. R. astr. Soc.*, **22,** 289–325.

Dziewonski, A., 1971b. Upper Mantle models from ' pure-path ' dispersion data, *J. geophys. Res.*, **76,** 2587–2601.

Dziewonski, A. & Landisman, M., 1970. Great circle Rayleigh and Love wave dispersion from 100 to 900 seconds, *Geophys. J. R. astr. Soc.*, **19,** 37–91.

Green, R. W. E. & Hales, A. L., 1968. The travel times of *P* waves to 30° in the Central United States and Upper Mantle structure, *Bull. seism. Soc. Am.*, **58,** 267–289.

Healy, J. H. & Warren, D. R., 1969. Explosion seismic studies in North America, in *The Earth's Crust and Upper Mantle*, ed. P. J. Hart, *Am. geophys. Union, Monograph* **13,** 208–220.

Helmberger, D. & Wiggins, R. A., 1971. Upper Mantle structure of Midwestern United States, *J. geophys. Res.*, **76,** 3229–3245.

Herrin, E. & Taggart, J., 1962. Regional variations in P_n velocity and their effect on the location of epicenters, *Bull. seism. Soc. Am.*, **52,** 1037–1046.

Huestis, S., Molnar, P. & Oliver, J., 1973. Regional S_n velocities and shear velocities in the Upper Mantle, *Bull. seism. Soc. Am.*, **63,** 469–475.

Iyer, H. M., Pakiser, L. C., Stuart, D. J. & Warren, D. H., 1969. Project Early Rise: Seismic probing of the Upper Mantle, *J. geophys. Res.*, **74,** 4409–4441.

Kanamori, H., 1970. Velocity and Q of Mantle waves, *Phys. Earth Planet. Int.*, **2,** 259–275.

Keilis-Borok, V. I. & Yanovskaya, T. B., 1967. Inverse problems of seismology (structural review), *Geophys. J. R. astr. Soc.*, **13,** 223–234.

Knopoff, L., 1972. Observation and inversion of surface-wave dispersion, *The Upper Mantle*, ed. A. R. Ritsema, Elsevier Publ. Co., Amsterdam, *Tectonophysics*, **13,** 497–519.

Knopoff, L., Berry, M. J. & Schwab, F. A., 1967. Tripartite phase velocity observations in laterally heterogeneous regions, *J. geophys. Res.*, **72,** 2595–2601.

Knopoff, L., Mueller, S. & Pilant, W. L., 1966. Structure of the Crust and Upper Mantle in the Alps from the phase velocity of Rayleigh waves, *Bull. seism. Soc. Am.*, **56,** 1009–1044.

Knopoff, L. & Schlue, J. W., 1972. Rayleigh wave phase velocities for the path Addis Ababa–Nairobi, in *East African Rifts*, ed R. W. Girdler, Elsevier Pub. Co., Amsterdam, *Tectonophysics*, **15,** 157–163.

Knopoff, L. & Schwab, F. A., 1968. Apparent initial phase of a source of Rayleigh waves, *J. geophys. Res.*, **73,** 755–760.

Lehmann, I., 1964. On the travel times of *P* as determined from nuclear explosions, *Bull. seism. Soc. Am.*, **54,** 123–139.

Madariaga, R. & Aki, K., 1972. Spectral splitting of toroidal-free oscillations due to lateral heterogeneity of the Earth's structure, *J. geophys. Res.*, **71,** 4421–4431.

McEvilly, T. V., 1964. Central U.S. Crust–Upper Mantle structure from Love and Rayleigh wave phase velocity inversion, *Bull. seism. Soc. Am.*, **54,** 1997–2015.

Pilant, W. L., 1967. Tectonic features of the Earth's crust and Upper Mantle, unpublished technical report prepared under United States Air Force contract No. AF 49 (638)–1534. (Available from the *Air Force Office of Scientific Research, Report No. AFOSR* 67–1797.)

Pilant, W. L. & Knopoff, L., 1964. Observations of multiple seismic events, *Bull. seism. Soc. Am.*, **54,** 19–39.

Downloaded from https://academic.oup.com/gji/article/36/3/515/585195 by guest on 21 August 2022

Press, F., 1968. Earth models obtained by Monte Carlo inversion, *J. geophys. Res.*, **73,** 5223–5234.

Press, F., 1969. The suboceanic Mantle, *Science*, **165,** 174–176.

Roy, R. F., Decker, E. R., Blackwell, D. D. & Birch, F., 1968. Heat flow in the United States, *J. geophys. Res.*, **73,** 5207–5221.

Satô, Y., 1955. Analysis of dispersed surface waves by means of Fourier transform I, *Bull. earthq. Res. Inst.*, **33,** 33–64.

Satô, Y., 1956. Analysis of dispersed surface waves by means of Fourier transform III. Analysis of practical seismogram of South Atlantic earthquake, *Bull. earthq. Res. Inst.*, **34,** 1931–1938.

Schwab, F., 1970. Surface-wave dispersion computations: Knopoff's method, *Bull. seism. Soc. Am.*, **60,** 1491–1520.

Schwab, F. & Knopoff, L., 1970. Surface-wave dispersion computations, *Bull. seism. Soc. Am.*, **60,** 321–366.

Simmons, G. & Roy, R. F., 1969. Heat flow in North America, in *The Earth's Crust and Upper Mantle*, ed. P. J. Hart, *Am. geophys. Union, Monograph* **13,** 78–81.

Toksöz, M. N. & Anderson, D. L., 1966. Phase velocities of long-period surface waves and structure of the Upper Mantle, *J. geophys. Res.*, **71,** 1649–1658.

Toksöz, M. N. & Ben-Menahem, A., 1963. Velocities of Mantle, Love and Rayleigh waves over multiple paths, *Bull. seism. Soc. Am.*, **53,** 741–781.

Downloaded from https://academic.oup.com/gji/article/36/3/515/585195 by guest on 21 August 2022